

**Determination of rare earth, major and trace elements in authigenic fraction of Andaman Sea (Northeastern Indian Ocean) sediments by Inductively Coupled Plasma-Mass Spectrometry**

R. Alagarsamy\*<sup>1,2</sup>, C.-F. You<sup>2</sup>, B. N. Nath<sup>1</sup> and A. V. Sijin Kumar<sup>1</sup>

1. National Institute of Oceanography, Council of Scientific and Industrial Research (CSIR), Dona Paula, Goa-403004, India

2. Earth Dynamic System Research Center, National Cheng Kung University, Tainan, Taiwan 70101, Republic of China

\*Corresponding author. Tel.: +91-832-2450436; Fax: +91-832-2450602.

E-mail address: alagar@nio.org

**Abstract**

Downcore variation of rare-earth elements (REEs) in the authigenic Fe-Mn oxides of a sediment core (covering a record of last ~40 kyr) from the Andaman Sea, a part of Indian Ocean show distinctive positive Ce and Eu anomalies. These positive Ce anomalies ( $Ce^*=1.1\sim 1.8$ ) are ascribed to be due to oxidation of deep sea sediments. The large positive Eu anomalies (i.e.,  $Eu^* > 1.8$  to 3.2) occur within a time span near the glacial/interglacial transition (~7,000-14,000 yr BP) which could be due to the past hydrothermal activity or to the effects arising from sea level changes. During glacial times, the Andaman Sea was almost completely isolated due to low sea level, leading to a reduction in sediment supply from the Ayeyarwady river. The variations of metal abundances (i.e., Ca, Al, Mn, and Fe) in the authigenic fraction provided independent information to evaluate the water column physicochemical changes during the glacial/interglacial transition period. The studied sediment core record changes in riverine inputs and reflect depositional changes related to sea level fluctuations and climatic events over the past 40 kyr in the Andaman Sea.

**Keywords:** Rare earth elements; trace elements; Fe-Mn oxyhydroxides; Andaman Sea.

## 1. Introduction

Rare earth elements (REEs) have been widely used as geochemical source fingerprints of rocks and sediments [1] and show small differences in their chemical properties, allowing only limited fractionation during weathering and sedimentation. Among the REEs, Ce and Eu present in two oxidation states, being, therefore, sensitive indicators of the redox conditions in the depositional environments.

Previous studies on sediment geochemistry [2,3], isotope composition [4], REE concentrations of surface waters [5,6] and monsoon variability of the Andaman Sea [7] were reported. However, the authigenic Fe-Mn oxides in the Andaman Sea sediments were not studied to understand the formation and delivery of this fraction. This study is the first investigation of REEs, major and trace element during Fe-Mn formation, as well as associated changes during the past 40 kyr in the Andaman Sea, a part of Indian Ocean. There are few REEs data available for the deep sea sediments of Andaman Sea, especially with systematic elemental contents along a long sediment core. In the present study, we report the REE distribution patterns in the leachates and to discuss the origin of the REEs and their elemental behavior during global sea-level changes over the past forty thousand years.

The Andaman Sea has a complex bottom topography that is characteristic of back-arc basins, being separated by the Andaman–Nicobar Ridge (Fig. 1). The submarine delta has been built by the outflow of the Irrawaddy and Salween rivers, which is connected to the eastern shallow shelves along the Malay Peninsula and the Malacca Strait, in the northern region. From the shelves, the sea bottom drops sharply into a large central and two smaller basins deeper than 2000 m extending along the north–south island arc. The maximum depth is 4180 m located at the south end of the central basin. As the sill depths of channels across the Andaman–Nicobar Ridge are shallower than 1800 m, the deep water of the Andaman Sea Basin is isolated from the Bay of Bengal and its water temperature remains as high as about 5°C at the bottom.

## 2. Materials and methods

Sediment core from Andaman Sea was recovered during O.R.V. Sagar Kanya cruise 168 (Fig. 1). Sediments were freeze-dried and ground for homogenization. The method applied for the extraction of the seawater-derived Fe–Mn oxy-hydroxide fraction was adopted from the previous method using hydroxylamine hydrochloride [8]. Samples were processed in acid-cleaned polypropylene centrifuge

tubes (15 mL) double rinses in deionised water (Milli-Q system). Carbonate was removed using a Na acetate buffer in a shaker using capped tubes in such a way to allow degassing of carbon dioxide during carbonate dissolution. Following centrifugation and double rinses in deionised water (Milli-Q system), the Fe–Mn oxy-hydroxide coatings was dissolved by leaching the samples for 2 h in a shaker at room temperature in a 1 M hydroxylamine hydrochloride (HH)–25% distilled acetic acid [8]. Concentrations of REEs, major and trace elements in the leach fractions were carried out in a Class 1000–10,000 clean room. A high resolution sector field ICP-MS (Thermo Fisher Scientific, Element 2) was used for determination of REEs, major and trace elements. Two introduction systems were employed in this study: 1) a low flow self-aspiration micro-concentric nebulizer coupled to a Cyclone-Scott tandem type spray chamber, and 2) a CETAC Aridus desolvation system incorporating a PFA micro-concentric nebulizer and heated PTFE spray chamber. The former instrument, which delivers stable signals, is for major and trace element analysis, and the latter instrument is responsible for reducing the polyatomic interferences during the determination of REEs. The concentrations of REEs were measured using the method explained by Chung et al. [9 and references therein]. Indium and rhenium were used as internal standards in order to correct potential instrumental drift. The international standard SLR-4 was also analyzed to check the validity of the measurement. The reagents used in the leaching and dissolution procedures are all high purity, double sub-boiled distilled acids. Hence, the blanks for all elements considered here are <<1% of the analyte.

The age model was constructed mainly by using Accelerator Mass Spectrometer (AMS)  $^{14}\text{C}$  data of planktic foraminiferal tests (*Globigerinoides ruber* and *Globigerinoides Saculifer*) of five horizons and calendar age calibration was based on the CalPal 2007 programme [10]. AMS dating was carried out at NOSAMS AMS facility at the Woods Hole Oceanographic Institute, USA. The AMS  $^{14}\text{C}$  ages were corrected for an 460 year reservoir age following Butzin et al. [11]. (The website link <http://radiocarbon.LDEO.columbia.edu>). Oxygen isotope stratigraphy of the core was established by correlation of the oxygen isotopic values of *Globigerinoides ruber* with the standard oxygen isotopic curve of Martinson et al. [12]. The ages for other horizons were assigned by interpolation/extrapolation of calibrated dates, assuming constant sedimentation rates.

### 3. Results and discussion

#### 3.1. Downcore distribution and variation of REE

All REEs and metals results are summarized in the Table 1. The shale-normalized REE patterns in the topmost ~1 m of the core shows that the light REE (La, Ce, Pr and Nd) content is lower than the shale resulting in a sample/shale ratio lower than 0.01 (Fig. 2). The shale-normalized REEs patterns shows that the authigenic fractions are enriched of MREE and HREE, indicative of their preferential removal from the seawater column over the LREE (Fig. 2). Between the MREE and HREE, the terrigenous contribution is enriched in the HREE than the MREE. REE concentrations gradually increase with the sample/shale ratio to show moderate MREE enrichment and no strong coefficient of determination ( $R^2$ ) between REE and Mn is seen (Table 2). It appears that the precipitation of oxy-hydroxides has a general tendency to develop MREE enrichment in the sediments [13].

#### 3.2. REE patterns

PAAS normalized REE patterns below 0.01 in the 0 to 110 cm sediment depth having low LREE and slightly higher HREE with Eu maxima in the MREE. Shale-normalized Eu varies between 0.01-0.1 in the sediment depth between 110 to 290 cm. REE patterns of the leach fractions have shown two distinctive features: (1) positive Ce and Eu anomalies (Fig. 3) and (2) MREE enrichment over LREE and HREE. Conversely, MREE enrichments in waters from a variety of rivers being tightly coupled with dissolved phosphate concentrations [14]. Hence the MREE enrichment could be caused by two different phases, either by leaching of phosphates or conversely, the precipitation of Fe–Mn oxy-hydroxides. It is reported that the REE budget during leaching of argillaceous sediments may be controlled by dissolution of authigenic apatite [15]. Contrary to that, there is no unambiguous indication that the MREE enrichment in porewaters is controlled by authigenic apatite [16]. It is difficult to fully rule out that part of the REE signal extracted during leaching of the Fe–Mn oxy-hydroxide fraction could be derived from contemporaneous leaching of authigenic apatite, but because of the preceding carbonate removal step. Authigenic apatite can be easily dissolved using dilute acetic acid [15]. As the very first chemical reagent used in this study for the extraction of the carbonate fraction, preceding the reductive leaching of Fe–Mn oxy-hydroxides, is Na acetate buffer containing acetic acid. Therefore, we attribute the MREE-enriched patterns mainly to be due to the release of REE from Fe–Mn oxy-hydroxide coatings (Fig. 2).

Cerium fractionation in the oceanic environment has been attributed to the oxidation of  $Ce^{3+}$  to  $Ce^{4+}$  as hydroxides and their subsequent uptake by Fe and Mn oxide particles. A strong positive Ce anomaly in the investigated samples suggests a highly oxidizing environment during their formation, similar to that noticed in ferromanganese nodules and crusts of hydrogenous origin [17, 18, 13].

Ce and possibly Eu show potential variations as a function of oxidation-reduction conditions in the sedimentary/oceanic environments. Only Ce and Eu deviate significantly from a line that declines toward the heavier rare earths. Cerium and La behave very coherently in their +3 oxidation states. The distribution of the La/Yb ratio in the sediments shows a marked increase toward the Younger Dryas to Heinrich events 2 (HE2) probably due to increased run-off from land, where the REEs are strongly associated with the oxide phase of the sediments. Perhaps with increased oxic conditions preferentially Ce was removed from the sediments towards the end of the HE2. Ce anomaly is mimicking the seawater REEs pattern [17]. The organisms extracting phosphate from oxic seawater show a negative Ce anomaly [19], whereas Fe oxide-rich oxic sediments, such as red clay, have a positive Ce anomaly [20]. Conversely, in suboxic seawater Ce-containing sediments are mobilized so that Ce is released into the water column [21].

Shale-normalized positive Eu anomalies were found either in water affected by eolian input [22] or in the hydrothermal solutions, as well as in sediments resulting from high temperature basalt alterations along mid-ocean ridges and back-arc spreading centres [23] or due to the contribution from in plagioclase content. The positive Eu anomalies in the Andaman sediments are more likely resulted from the hydrothermal input [2] as there is only negligible long-range transported eolian source. The main land surrounding Andaman Sea (Myanmar, Thailand and Andaman Islands) is well vegetated and has a rather humid climate [2].  $Eu^{3+}$  to  $Eu^{2+}$  valency changes can take place at high temperatures ( $>200^{\circ}C$ ) during redox transformations and low oxidation-reduction potentials (pH 2-4) [2 and references therein]. By using REE data in pore water from Buzzards Bay sediments, the positive Eu anomalies were found to be attained in sediments within a time span of 10,000-12,000 yr of diagenetic history [2 and references therein] and in the present study shown at  $\sim 7,000$ -14,000 yr of time span (Fig. 3), covering Holocene, Younger Dryas and Bølling/Allerød. The Andaman Sea sediment core covers a length of 290 cm with an average sedimentation rate of  $\sim 10$  cm kyr<sup>-1</sup>.

### 3.3. Ca, Fe and Mn enrichment in the authigenic fraction

There is a sudden increase of Ca at the depth ~100-200 cm and remains high during the HE1 period where also flagged by the onset of higher Al, P, Ti and Fe in Andaman Sea sediments (Fig. 4). These sediments have higher CaO contents and Sr reflecting the presence of higher biogenic carbonate content due to pelagic deposition [2]. Due to the presence of high Ca and Mn during LGM ~20 ka BP, significant Mn and Ca accumulations are seen down to 100-200 cm sediment depth. The diagenetically supplied dissolved Mn may accumulate in a pool at the seawater-sediment interface and be involved in the transformation into the carbonate phase when oxic bottom water reaches these pools. The carbonate then settles on the seafloor and creates layers of rhodochrosite [24]. A significant observation is that the Ca normalized profile showed enrichments of Fe, Mg, Ba and P concentrations until HE1 ~14 ka BP, while enrichment of Mn is observed upto 4 ka BP during the marine isotope stage 1 (MIS 1). The values for Mn, Fe, Mg, Ba and P are below detection in the younger sedimentary layer upto 33 ka BP and downlain by older sedimentary layer with higher Fe, Mg, Ba and P content which corresponds to HE4. These observations suggest that maximal transgressive periods would lead to elevated Ca-Mn in sediments due to increased deposition of rhodochrosite [24]. Low sea level stands, at the end of a transgressive phase, a lower rhodochrosite signal would be formed in the sediments, while there is sufficient dissolved Mn and/ or increased alkalinity to produce authigenic rhodochrosite in the Andaman Sea.

Within MIS, variations in the authigenic fraction Al, Ca, P, Ti and Fe content of sediments show a strong relation to events recorded in the Greenland ice core and also similar to the bulk Fe, Ti and Ca content of Cariaco Basin in the tropical Atlantic. Higher Fe and Ti values are closely associated with sediments deposited during the interstadials, whereas Ca values show the opposite trend which agree with the findings of tropical Atlantic [25]. Although the Fe behavior alone might be attributed to the parallel redox changes in the sediment, Ti behavior, which is redox-insensitive, shows an identical downcore pattern. Hence, Fe and Ti variations in the Andaman Basin are not diagenetically controlled.

On glacial-interglacial time scales, TOC fluctuations could be interpreted to reflect the first-order history of export productivity in the Andaman Basin, with sea level playing an important role in modulating that production. During glacials, lowered sea levels would have increasingly isolated the Andaman Basin and restricted input of nutrient-rich subsurface waters, thus limiting production and reducing O<sub>2</sub>

consumption from the remineralization of sinking organic detritus. In contrast, high interglacial sea levels increase the supply of nutrients from the open ocean stimulating productivity and contributing to the anoxic depositional conditions that prevailed at these times. Presence of mid-depth intense OMZ between 150 - 800 m water depths in the Andaman Sea is also reported [26]. We interpret these results to indicate both higher biological productivity and increased terrigenous input to the Andaman Basin during interstadial times. TOC (>1%) and Ba (>20 µg/g) values are increased during interstadial times (Fig. 5). The sediments of Andaman Sea are invariably fine-grained derived from Myanmar Rivers (Irrawaddy, Salween) and are responsible for the organic enrichments along the western Andaman Sea [27]. High TOC observed during the isotopic stages 2 and 3 are probably due to the enhanced productivity.

The climate variability during marine oxygen isotope stages 2 and 3 was characterized by an alternation of warm and cold periods (stadials/ interstadials), which lasted up to several thousand years in the Andaman Sea. Are the millennial-scale variations for the glacial interval also a reflection of changing surface productivity? At first glance, the low Ca contents of sediments deposited during interstadials (Fig. 4) might seem to indicate low productivity of calcareous plankton. However, preliminary foraminiferal data in fact suggest the opposite, with high abundances of the productivity indicator *G. bulloides* found in the laminated intervals. Increased carbonate dissolution, another possibility for explaining low interstadial Ca values, is ruled out by the fact that aragonitic pteropods are common throughout the sequence and foraminiferal preservation is excellent. The striking inverse relation between Ca and Fe in these sediments instead suggests that dilution plays the major role in their respective downcore distributions.

The maximum abundance of *G. bulloides* during glacial interglacial transition and especially Younger Dryas indicate intensification of upwelling resulted by strong summer monsoon in Andaman Sea (Fig. 5). Earlier studies from Andaman Sea showed that summer monsoon was stronger during B/A and Holocene and weaker during glacial [6] which is good agreement with our *G. bulloides* record. Sediment trap data and laboratory experiments suggest that *G. bulloides* thrives mainly between 0 and 100 m depth in the surface mixed layer above the thermocline, in the upwelling environments, where phytoplankton density and prey abundance are high [28 and references therein]. In general, Andaman Sea was characterized by poor summer monsoon induced upwelling and productivity during glacial than Holocene.

The Andaman Basin is an enclosed region in the northeastern Indian Ocean with its deep water below ~ 1800 m almost isolated with respect to horizontal ventilation by the Andaman–Nicobar Islands separating it from the Bay of Bengal and show negligible variation with depth in the waters below 1300 m, indicating a well-mixed water mass underlain with a young crust and is known for its high heat flow, which also could contribute to the high vertical mixing [29]. Nozaki and Alibo [7] observed preferential scavenging of lighter rare earth elements (REE) from water column at the bottom boundary of Andaman Sea Basin and homogenized dissolved REE concentration in addition to other parameters in vertical profiles of deep waters below 1800 m in Andaman Sea and attributed it to rapid turbulent mixing, probably induced due to the complex bottom topography.

Salinity variation can cause significant seawater Ca to be precipitated [30]. It is clearly seen in the figure 4 that REE contents in the sediments at depths 290 to 225 cm decrease significantly, possibly influenced by freshwater input during de-glaciation. It is clearly evidenced from the previous findings that rapid climate change during the last deglaciation and Holocene included substantial hydrologic changes in the Indian Ocean Monsoon system that were coherent with the larger Asian monsoon [6].

A minor fraction of the REE is possible carried by a phosphate phase, shown by an insignificant coefficient of determination ( $R^2$ ) with P (Table 2). This phosphate phase may not be biogenic apatite due to a lack of strong coefficient of determination ( $R^2$ ) between Ca and P (Table 2;  $R^2 = 0.08$ ). Fe and Ca are correlated insignificantly with Al suggesting aluminosilicates (e.g. clays) play a minor role in controlling the chemical composition of oxy-hydroxides fraction. Unlike other elements, Ca shows distinct and significant coefficient of determination ( $R^2$ ) in sections of 0-110, 120-230, and 240-290 cm.

Generally phosphate and smectite are characterized by a negative Ce-anomaly and contain high REE abundance [20 and references therein]. The lack of negative Ce-anomaly in this sediment core reveals that minor retention of REEs in phosphate and smectite. Fe-rich smectites formed by the weathering of submarine volcanic rocks and glass show a positive Ce-anomaly whereas Fe-rich smectites formed by early diagenesis have negative Ce-anomaly [31 and references therein]. Authigenic Fe-rich smectite is formed commonly by the interaction between iron oxy-hydroxide and biogenic opal [32].

Mineralogical and geochemical studies confirm the contribution of Fe from Irrawaddy and other Myanmar rivers and local basaltic sources. The geochemical data on Fe, Mn, Ba and P are used further to differentiate between the diagenetic and hydrothermal signatures (Fig. 4, 5). Mn showed significant enrichment (1-4%) in the top 12 cm and low Mn content in the deeper samples due to clay mineral Mn



or carbonate-Mn [2] and suggested that Mn enrichment in the upper sediment are due to hydrothermal process which played a major role. In the present study, higher level of Ba, which is a productivity proxy, is observed upto ~14 ka BP during B/A but reduced Ba content during 15-40 ka BP (MIS 2-3) due to the “Late glacial” interval suggesting a near collapse of productivity [6]. Downward metal concentration varied similarly to those observed for P (between ~20 and 80 µg/g), with lower concentrations occurring during glacial intervals (H1) and higher concentrations during interglacial intervals (Fig. 4). P is highly correlated with Mg, Al and Fe (Table 2).

#### **4. Conclusions**

This study focuses on detailed analyses of the major, trace and REE's in the authigenic fraction of Andaman Sea sediment. The downcore distribution of REEs in the Andaman Sea sediments showed a distinctive positive Ce and Eu anomalies in the authigenic Fe-Mn oxides fraction. The positive Ce anomalies are ascribed to be due to oxidation of deep sea sediments and the positive Eu anomalies occur within a time span (~7,000-14,000 yr) during the glacial/interglacial transition. The metal abundances in the authigenic fraction provided independent data to evaluate glacial/interglacial fluctuations in the hydrographic conditions and the variations are interpreted as changes in riverine inputs and reflect sedimentation conditions related to sea level fluctuations and climatic events during the past 40 kyr. REEs patterns are typical of Mn oxides and suggest that Mn is the predominant oxide/oxy-hydroxide form in the surficial sediments.  $Ce_{anomalies}$ , Ca, Al, P, Mn and Fe concentrations increased during the time span 15-40 ka BP and Eu decreased suggesting the metal abundances in the late glacial period in the older sedimentary layer compared to the younger sediments. The enrichment of Ba, TOC and *G. Bulloides* reflected the biological productivity of the overlying waters.

#### **Acknowledgements**

The author R.A would like to thank National Science Council, Taiwan for the financial support and Director, NIO for permission. Yu-Hui and Bo are thanked for their help in the laboratory to carry out these analyses. R.A is grateful to His Holiness Sri Sri Ravishankar for grace, support and encouragement. This study is supported by grants from NSC and MOE to YCF. Ministry of Earth Sciences (formerly Department of Ocean Development, Government of India) is thanked for the ship time. Officers, scientists and crew of SK-168 are thanked for their help during the cruise. Ms. Naman helped in sampling onboard and processing in shore laboratory and Ms. Supriya Karapurkar for oxygen isotope analyses. Expenditure towards oxygen isotope analyses and AMS dating were largely met from CSIR networked project on Mid-oceanic Ridge studies (COR-006). This is NIO contribution no.

## References

- [1] P. Henderson, Rare earth element geochemistry, Elsevier, (1984) 343 p.
- [2] S. Kurian, B.N. Nath, V. Ramaswamy, D. Naman, T.G. Rao, K.A. Kamesh Raju, K. Selvaraj, C.T.A. Chen, Possible detrital, diagenetic and hydrothermal sources for Holocene sediments of the Andaman backarc basin, *Mar. Geol.* 247 (2008) 178–193.
- [3] H.M. Stoll, D. Vance, A. Arevalos, Records of the Nd isotope composition of seawater from the Bay of Bengal: Implications for the impact of Northern Hemisphere cooling on ITCZ movement, *Earth Planet. Sci. Lett.* 255 (2007) 213-228.
- [4] C. Colin, L. Turpin, J. Bertaux, A. Desprairies, C. Kissel, Erosional history of the Himalayan and Burman ranges during the last two glacial–interglacial cycles. *Earth Planet. Sci. Lett.* 171 (1999) 647-660.
- [5] H. Amakawa, D.S. Alibo, Y. Nozaki, Nd isotopic composition and REE pattern in the surface waters of the eastern Indian Ocean and its adjacent seas, *Geochim. Cosmochim. Acta* 64 (2000) 1715-1727.
- [6] H. Rashid, B. P. Flower, R. Z. Poore, T. M. Quinn, A ~25 ka Indian Ocean monsoon variability record from the Andaman Sea, *Quarter. Sci. Rev.* 26 (2007) 2586-2597.
- [7] Y. Nozaki, D.S. Alibo, Importance of vertical geochemical processes in controlling the oceanic profiles of dissolved rare earth elements in the northeastern Indian Ocean. *Earth Planet. Sci. Lett.* 205 (2003) 155-172.
- [8] R. Chester, M.J. Hughes, A chemical technique for the separation of ferromanganese minerals, carbonate minerals and adsorbed trace elements for pelagic sediments, *Chem. Geol.* 2 (1967) 249–262.
- [9] C.H. Chung, C.F. You, H.Y. Chu, Weathering sources in the Gaoping (Kaoping) river catchments, southwestern Taiwan: Insights from major elements, Sr isotopes, and rare earth elements. *J. Mar. Syst.* 76, (2009), 433-443.
- [10] B. Weninger, O. Jöris, U. Danzeglocke. CalPal-2007 Cologne Radiocarbon Calibration & Palaeoclimate Research Package, (2007). <http://www.calpal.de>
- [11] M. Butzin, M. Prange, G. Lohmann, Radiocarbon simulations for the glacial ocean: the effects of wind stress, Southern Ocean sea ice and Heinrich events. *Earth Planet. Sci. Lett.* 235 (2005) 45-61.

- [12] D.G. Martinson, N.G. Pisias., J.D. Hays, J. Imbrie, T.C. Jr. Moore, N.J. Shackleton. Age dating and the orbital theory of the ice ages: development of a high-resolution 0 to 300,000-year chronostratigraphy. *Quat. Res.* 27 (1987) 1-29.
- [13] C. Yingchun, L. Jihua, R. Xiangwen, S. Xuefa, Geochemistry of rare earth elements in cobalt-rich crusts from the Mid-Pacific M seamount, *J. Rare Earths* 27 (2009), 169-176.
- [14] R. E. Hannigan, E.R. Sholkovitz, The development of middle rare earth element enrichments in freshwaters: weathering of phosphate minerals, *Chem. Geol.* 175 (2001) 495–508.
- [15] M. Ohr, A. N. Halliday, D.R. Peacor, Mobility and fractionation of rare earth elements in argillaceous sediments: implications for dating diagenesis and low-grade metamorphism, *Geochim. Cosmochim. Acta.* 58 (1994) 289–312.
- [16] B.A. Haley, G.P. Klinkhammer, J. McManus, Rare earth elements in pore waters of marine sediments, *Geochim. Cosmochim. Acta* 68 (2004) 1265–1279.
- [17] H. Elderfield, C.J. Hawkesworth, M.J. Greaves, S.E. Calvert, Rare-earth element geochemistry of oceanic ferromanganese nodules and associated sediments. *Geochim. Cosmochim. Acta.* 45 (1981) 513-528.
- [18] B.N. Nath, I. Roelandts, M. Sudhakar, W. L. Plueger, V. Balaram, Cerium anomaly variations in ferromanganese nodules and crusts from the Indian Ocean, *Mar. Geol.* 120 (1994) 385-400.
- [19] J. Wright, H. Schrader, W. T. Holser, Paleoredox variations in ancient oceans recorded by rare earth elements in fossil apatite, *Geochim. Cosmochim. Acta* 51 (1987) 631-644.
- [20] J. Thomson, M. S. N. Carpenter, S. Colley, T. R. S. Wilson, H. Elderfield, H. Kennedy, Metal accumulation rates in northwest Atlantic pelagic sediments, *Geochim. Cosmochim. Acta* 48 (1984) 1935-1948.
- [21] E.R. Sholkovitz, D. L. Schneider, Cerium redox cycles and rare earth elements in the Sargasso Sea, *Geochim. Cosmochim. Acta* 55 (1991) 2737-2743.
- [22] H. Elderfield, The oceanic chemistry of the rare earth elements, *Philos. Trans. R. Soc. Lond. A* 325 (1988) 105–126.
- [23] Michard, F. Albarède, G. Michard, J.F. Minster, J.L. Charlou, Rare earth elements and uranium in high temperature solutions from East Pacific Rise hydrothermal vent field (13°N), *Nature* 303 (1983) 795–797.
- [24] H. Kunzendorf, B. Larsen, A 200–300 year cyclicity in sediment deposition in the Gotland Basin, Baltic Sea, as deduced from geochemical evidence, *App. Geochem.* 17 (2002) 29-38.

- [25] L.C. Peterson, G. H. Haug, K. A. Hughen, U. Röhl, Rapid Changes in the Hydrologic Cycle of the Tropical Atlantic During the Last Glacial, *Science* 290 (2000) 1947-1951.
- [26] R. Sen Gupta, C. Moraes, M.D. George, T.W. Kureishy, R.J. Noronha, S.P. Fondekar, Chemistry and hydrography of the Andaman Sea, *Indian J Mar Sci.* 10 (1981) 228–233.
- [27] V. Ramaswamy, B. Gaye, P.V. Shirodkar, P.S. Rao, A.R. Chivas, D. Wheeler, Swe Thwin, Distribution and sources of organic carbon, nitrogen and their isotopic signatures in sediments from the Ayeyarwady (Irrawaddy) continental shelf, northern Andaman Sea. *Mar. Chem.* 111 (2008) 137-150.
- [28] M. Mohtadi, D. Hebbeln, M. Marchant, Upwelling and productivity along the Peru–Chile Current derived from faunal and isotopic compositions of planktic foraminifera in surface sediments, *Mar. Geol.* 216 (2005) 107-126.
- [29] K. Dutta, R. Bhushan, B.L.K. Somayajulu, Rapid vertical mixing rates in deep waters of the Andaman Basin, *Sci. of the Total Environ.* 384 (2007) 401-408.
- [30] C. Christiansen, H. Kunzendorf, H.R. Tychsen, CaCO<sub>3</sub> in sediments from the North Sea-Baltic Sea transition: Signals of high salinity? Proceed. 3<sup>rd</sup> Marine Geological Conf.- The Baltic. Prace Państwowego Instytutu Geologicznego, Warszawa, (1995) 151-154.
- [31] B.N. Nath, V. Balaram, M. Sudhakar, W. L. Plueger, Rare earth element geochemistry of ferromanganese deposits from the Indian Ocean, *Mar. Chem.* 38 (1992) 185-208.
- [32] M. Lyle, J. Dymond, G.R. Heath, Copper–nickel enriched ferromanganese nodules and associated crusts from the Baur Basin, northwest Nazca plate, *Earth Planet. Sci. Lett.* 35 (1977) 55–64.

## Figure Caption

Figure 1. Location of the sampling sites during O.R.V. Sagar Kanya cruise 168 (#GC-1) (Modified from Kamesh Raju et al., 2004)

Figure 2. Plot showing the variation of REE patterns in the Andaman Sea sediment core

Figure 3. Plot showing the downcore variation of La, Nd, Yb, La/Yb, Ce and Eu anomalies in the authigenic fraction with age in the Andaman Sea sediment core

Figure 4. Plot showing the downcore variation of Ba, P, Ca, Al, Ti, Mn and Fe in the authigenic fraction with age in the Andaman Sea sediment core

Figure 5. Plot showing the downcore variation of Ba, Eu anomaly, *G.bulloides* and TOC (%) in the the authigenic fraction with age in the Andaman Sea sediment core

Table

Table 1 Selected major and trace element concentrations ( $\mu\text{g/g}$ ) in the Fe-Mn oxy-hydroxide leach fraction

Table 2 Coefficient of determination ( $R^2$ ) for the measured elements in the Andaman Sea sediment core #GC-1 ( $R^2 > 0.35$ ,  $p < 0.05$ ,  $n = 30$ , bold figures are significant)

Table 1

Depth (cm)	Ba	P	Mg	Ca	Al	Ti	Mn	Fe	La	Ce	Pr	Nd	Sm	Eu	Gd	Tb	Dy	Ho	Er	Tm	Yb	Lu
0-2	36.3	23.8	228	227	197	1.9	2638	392	0.27	0.83	0.07	0.32	0.08	0.04	0.09	0.01	0.07	0.01	0.04	0.01	0.03	0.01
8-10	26	21.5	234	261	172	1.9	1538	285	0.30	0.81	0.08	0.37	0.09	0.03	0.10	0.02	0.08	0.02	0.04	0.01	0.04	0.01
18-20	19.2	23.3	268	369	167	1.8	960	210	0.25	0.62	0.07	0.31	0.08	0.03	0.09	0.01	0.07	0.01	0.04	0.01	0.03	0.01
28-30	20.5	21	231	308	168	1.9	967	202	0.27	0.68	0.07	0.34	0.09	0.03	0.09	0.02	0.08	0.02	0.04	0.01	0.03	0.01
38-40	22.3	16.7	181	175	80	1.8	61	76	0.16	0.42	0.05	0.24	0.06	0.03	0.07	0.01	0.05	0.01	0.03	0.00	0.02	0.00
48-50	50	14.2	163	180	94	2.1	44	162	0.14	0.39	0.05	0.21	0.06	0.04	0.06	0.01	0.05	0.01	0.02	0.00	0.02	0.00
57-60	26.7	17.3	150	139	58	1.8	36	67	0.12	0.32	0.04	0.18	0.05	0.02	0.05	0.01	0.04	0.01	0.02	0.00	0.02	0.00
67-70	40.4	14.7	176	106	77	1.8	33	88	0.13	0.36	0.04	0.19	0.05	0.03	0.05	0.01	0.04	0.01	0.02	0.00	0.02	0.00
77-80	33.1	14.7	135	106	63	1.7	35	74	0.10	0.29	0.03	0.16	0.04	0.03	0.04	0.01	0.04	0.01	0.02	0.00	0.01	0.00
87-90	26	14.7	182	131	79	1.8	48	123	0.12	0.34	0.04	0.17	0.04	0.02	0.05	0.01	0.04	0.01	0.02	0.00	0.02	0.00
97-100	26.5	16	238	189	88	1.7	84	129	0.12	0.35	0.04	0.17	0.05	0.02	0.05	0.01	0.04	0.01	0.02	0.00	0.02	0.00
107-110	37.6	15.5	195	140	71	1.8	73	119	0.11	0.34	0.04	0.16	0.04	0.03	0.04	0.01	0.03	0.01	0.02	0.00	0.01	0.00
117-120	9.9	39.9	638	14446	204	8.6	447	158	1.24	3.54	0.34	1.53	0.37	0.10	0.41	0.07	0.33	0.07	0.18	0.02	0.14	0.03
127-130	22.9	44.1	640	12345	194	10	366	202	1.49	4.28	0.41	1.87	0.46	0.13	0.50	0.08	0.38	0.08	0.19	0.03	0.15	0.03
137-140	5.6	44.7	658	14896	191	12.1	410	182	1.60	4.68	0.45	1.98	0.49	0.13	0.53	0.09	0.42	0.09	0.21	0.03	0.17	0.03
147-150	8.4	28.9	565	9666	147	6.8	1060	174	1.60	4.79	0.43	1.95	0.48	0.12	0.51	0.08	0.39	0.08	0.20	0.03	0.15	0.03
157-160	7.3	41.5	659	10426	158	6	2527	227	1.60	5.00	0.44	1.91	0.47	0.12	0.51	0.08	0.38	0.08	0.19	0.03	0.15	0.03
167-170	18.8	29.8	490	4967	153	4.9	1019	232	1.00	3.14	0.28	1.28	0.31	0.08	0.34	0.05	0.25	0.05	0.12	0.02	0.10	0.02
177-180	9.8	40.4	650	9752	210	6.1	1216	364	1.66	5.12	0.44	1.91	0.47	0.12	0.50	0.08	0.38	0.08	0.19	0.03	0.15	0.03
187-190	21	32.7	449	11536	149	5.9	679	203	1.68	5.14	0.45	1.94	0.48	0.12	0.51	0.08	0.39	0.08	0.20	0.03	0.15	0.03
197-200	6.6	25.1	460	9063	130	11.2	476	176	1.43	4.64	0.39	1.66	0.40	0.10	0.44	0.07	0.32	0.07	0.16	0.02	0.13	0.02
205-210	11	36.1	452	9295	174	6.5	309	208	1.58	5.07	0.43	1.85	0.45	0.12	0.50	0.08	0.38	0.08	0.19	0.03	0.15	0.03
215-220	5.7	48	679	12407	177	7.6	1147	204	1.68	5.19	0.46	2.00	0.50	0.13	0.55	0.09	0.43	0.09	0.22	0.03	0.17	0.03
225-230	7.3	34.4	538	9792	145	6.7	978	191	1.29	4.00	0.35	1.54	0.39	0.10	0.43	0.07	0.33	0.07	0.16	0.02	0.13	0.02
235-240	15.1	49.2	477	1781	206	2.3	478	356	0.40	1.27	0.12	0.57	0.15	0.04	0.17	0.03	0.12	0.02	0.06	0.01	0.05	0.01
245-250	9	68.1	601	1908	291	2	525	553	0.49	1.75	0.16	0.73	0.19	0.05	0.21	0.03	0.15	0.03	0.08	0.01	0.06	0.01
255-260	30	67.4	659	2747	295	2.5	462	501	0.57	1.97	0.18	0.81	0.22	0.06	0.24	0.04	0.17	0.03	0.08	0.01	0.07	0.01
265-270	28.8	65	726	5141	317	4.5	810	514	0.81	2.61	0.25	1.16	0.30	0.09	0.33	0.05	0.24	0.05	0.12	0.02	0.10	0.02
275-280	9.1	77.2	725	2389	305	2.3	901	726	0.43	1.42	0.14	0.66	0.18	0.05	0.20	0.03	0.15	0.03	0.07	0.01	0.06	0.01
285-290	5.2	77.7	738	2001	280	1.9	816	625	0.40	1.33	0.13	0.63	0.17	0.05	0.18	0.03	0.13	0.03	0.07	0.01	0.05	0.01

Table 2

	Ba	P	Mg	Ca	Al	Ti	Mn	Fe	La	Ce	Pr	Nd	Sm	Eu	Gd	Tb	Dy	Ho	Er	Tm	Yb	Lu	
Ba	1.00																						
P	0.26	1.00																					
Mg	<b>0.49</b>	<b>0.76</b>	1.00																				
Ca	<b>0.39</b>	0.08	<b>0.45</b>	1.00																			
Al	0.17	<b>0.85</b>	<b>0.63</b>	0.05	1.00																		
Ti	0.31	0.03	0.31	<b>0.86</b>	0.01	1.00																	
Mn	0.07	0.04	0.09	0.03	0.12	0.01	1.00																
Fe	0.07	<b>0.76</b>	<b>0.38</b>	0.01	<b>0.82</b>	0.03	0.11	1.00															
La	<b>0.42</b>	0.08	<b>0.45</b>	<b>0.91</b>	0.06	<b>0.77</b>	0.09	0.00	1.00														
Ce	<b>0.43</b>	0.10	<b>0.47</b>	<b>0.88</b>	0.07	<b>0.74</b>	0.09	0.00	<b>0.99</b>	1.00													
Pr	<b>0.43</b>	0.11	<b>0.50</b>	<b>0.91</b>	0.08	<b>0.77</b>	0.08	0.00	1.00	<b>0.99</b>	1.00												
Nd	<b>0.44</b>	0.12	<b>0.52</b>	<b>0.91</b>	0.09	<b>0.77</b>	0.08	0.00	<b>0.99</b>	<b>0.99</b>	1.00	1.00											
Sm	<b>0.45</b>	0.14	<b>0.55</b>	<b>0.91</b>	0.10	<b>0.76</b>	0.08	0.00	<b>0.99</b>	<b>0.99</b>	1.00	1.00	1.00										
Eu	0.35	0.12	<b>0.51</b>	<b>0.92</b>	0.09	<b>0.78</b>	0.08	0.00	<b>0.97</b>	<b>0.96</b>	<b>0.98</b>	<b>0.98</b>	<b>0.98</b>	1.00									
Gd	<b>0.45</b>	0.14	<b>0.56</b>	<b>0.91</b>	0.11	<b>0.76</b>	0.08	0.00	<b>0.99</b>	<b>0.99</b>	<b>0.99</b>	1.00	1.00	<b>0.98</b>	1.00								
Tb	<b>0.45</b>	0.13	<b>0.54</b>	<b>0.93</b>	0.09	<b>0.79</b>	0.07	0.00	<b>0.98</b>	<b>0.98</b>	<b>0.99</b>	<b>0.99</b>	<b>0.99</b>	<b>0.97</b>	<b>0.99</b>	1.00							
Dy	<b>0.45</b>	0.13	<b>0.54</b>	<b>0.93</b>	0.09	<b>0.78</b>	0.08	0.00	<b>0.99</b>	<b>0.98</b>	<b>0.99</b>	1.00	1.00	<b>0.98</b>	1.00	<b>0.99</b>	1.00						
Ho	<b>0.45</b>	0.11	<b>0.51</b>	<b>0.94</b>	0.08	<b>0.80</b>	0.07	0.00	<b>0.98</b>	<b>0.98</b>	<b>0.99</b>	<b>0.99</b>	<b>0.99</b>	<b>0.98</b>	<b>0.99</b>	<b>0.99</b>	<b>0.99</b>	1.00					
Er	<b>0.46</b>	0.12	<b>0.53</b>	<b>0.94</b>	0.09	<b>0.78</b>	0.08	0.00	<b>0.98</b>	<b>0.98</b>	<b>0.99</b>	<b>0.99</b>	<b>0.99</b>	<b>0.98</b>	<b>0.99</b>	<b>0.99</b>	1.00	<b>0.99</b>	1.00				
Tm	<b>0.42</b>	0.13	<b>0.51</b>	<b>0.82</b>	0.14	<b>0.66</b>	0.18	0.01	<b>0.93</b>	<b>0.92</b>	<b>0.93</b>	<b>0.94</b>	<b>0.94</b>	<b>0.92</b>	<b>0.94</b>	<b>0.92</b>	<b>0.94</b>	<b>0.92</b>	<b>0.94</b>	1.00			
Yb	<b>0.45</b>	0.13	<b>0.54</b>	<b>0.94</b>	0.10	<b>0.79</b>	0.08	0.00	<b>0.98</b>	<b>0.97</b>	<b>0.99</b>	<b>0.99</b>	<b>0.99</b>	<b>0.98</b>	<b>0.99</b>	<b>0.99</b>	1.00	<b>0.99</b>	<b>0.99</b>	<b>0.93</b>	1.00		
Lu	<b>0.43</b>	0.13	<b>0.53</b>	<b>0.87</b>	0.15	<b>0.69</b>	0.16	0.01	<b>0.93</b>	<b>0.91</b>	<b>0.93</b>	<b>0.94</b>	<b>0.93</b>	<b>0.92</b>	<b>0.93</b>	<b>0.92</b>	<b>0.94</b>	<b>0.93</b>	<b>0.95</b>	<b>0.98</b>	<b>0.94</b>	1.00	



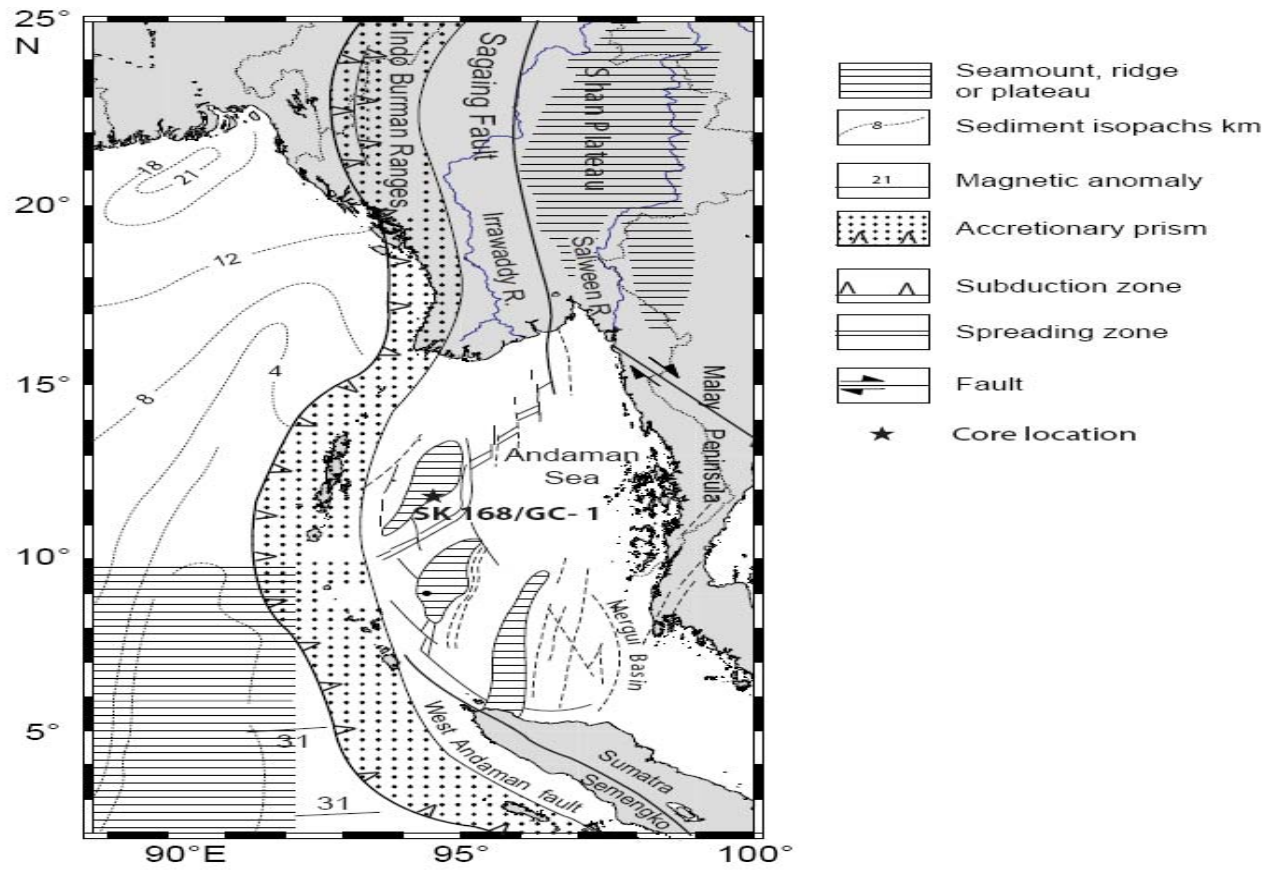


Fig. 1

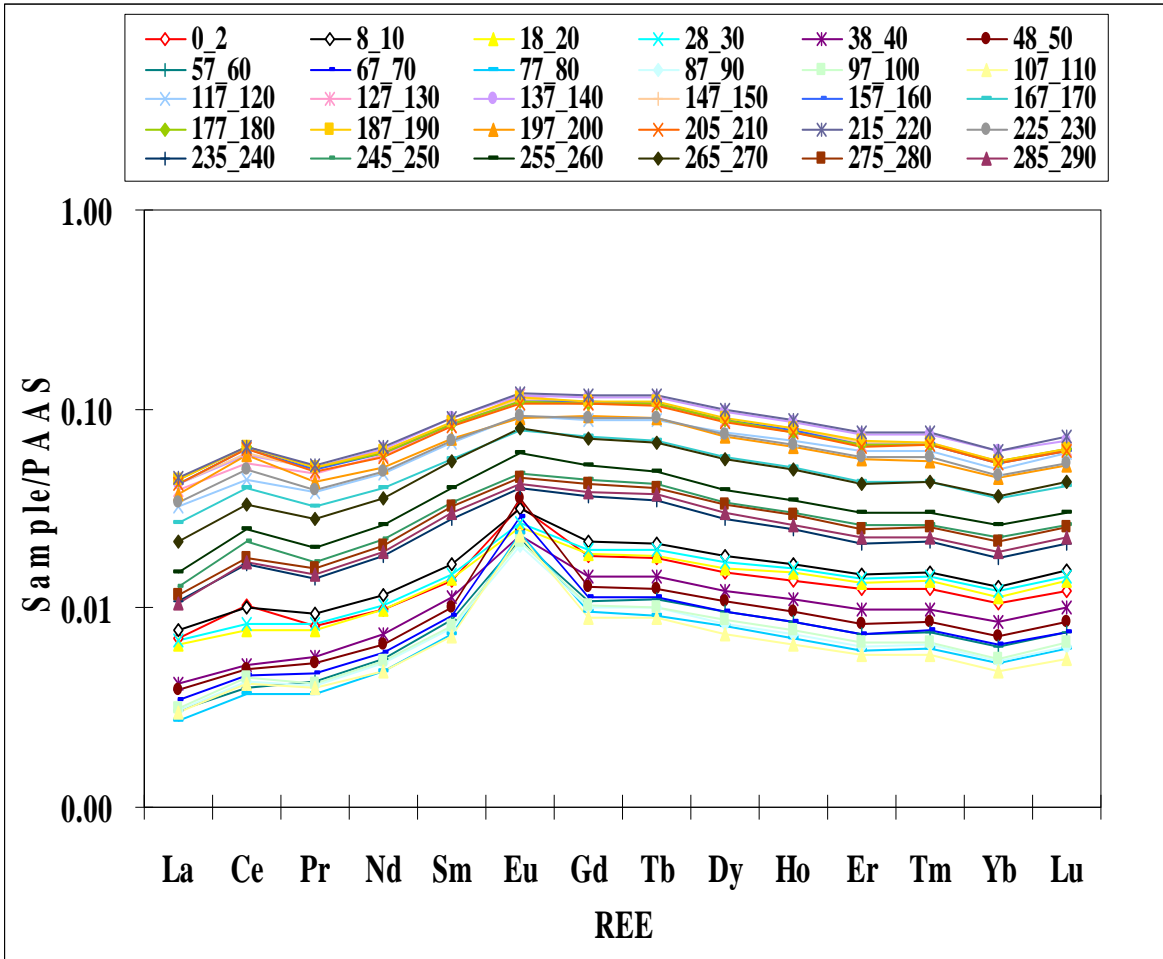


Fig. 2

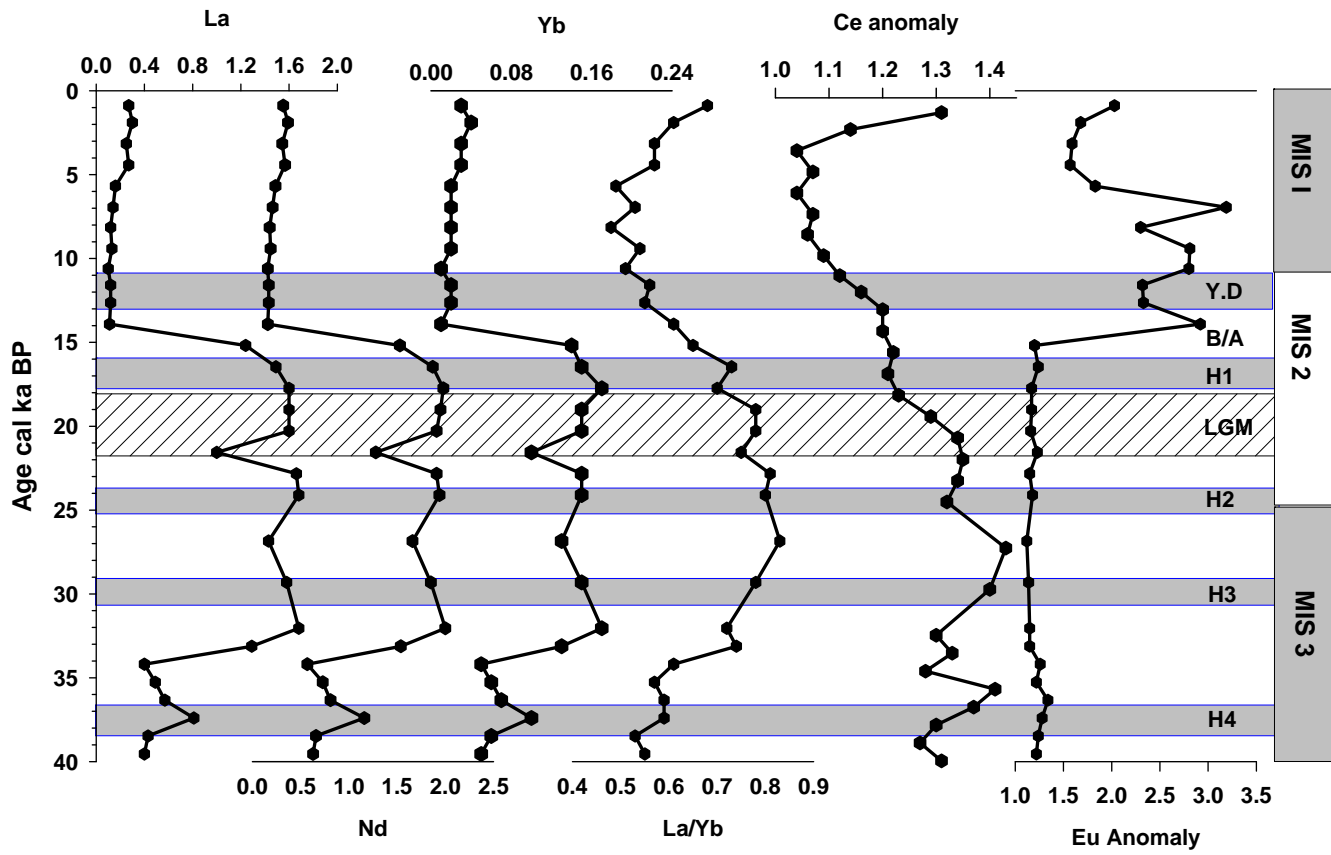


Fig. 3

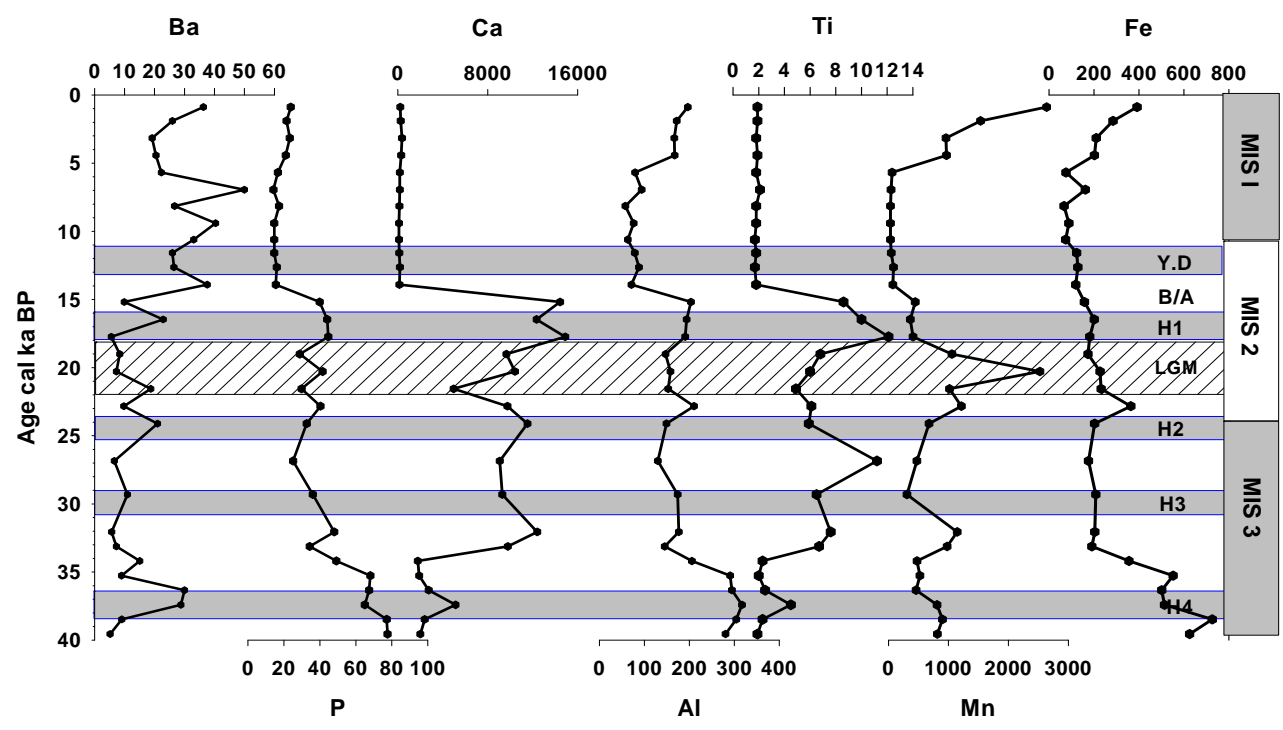


Fig. 4

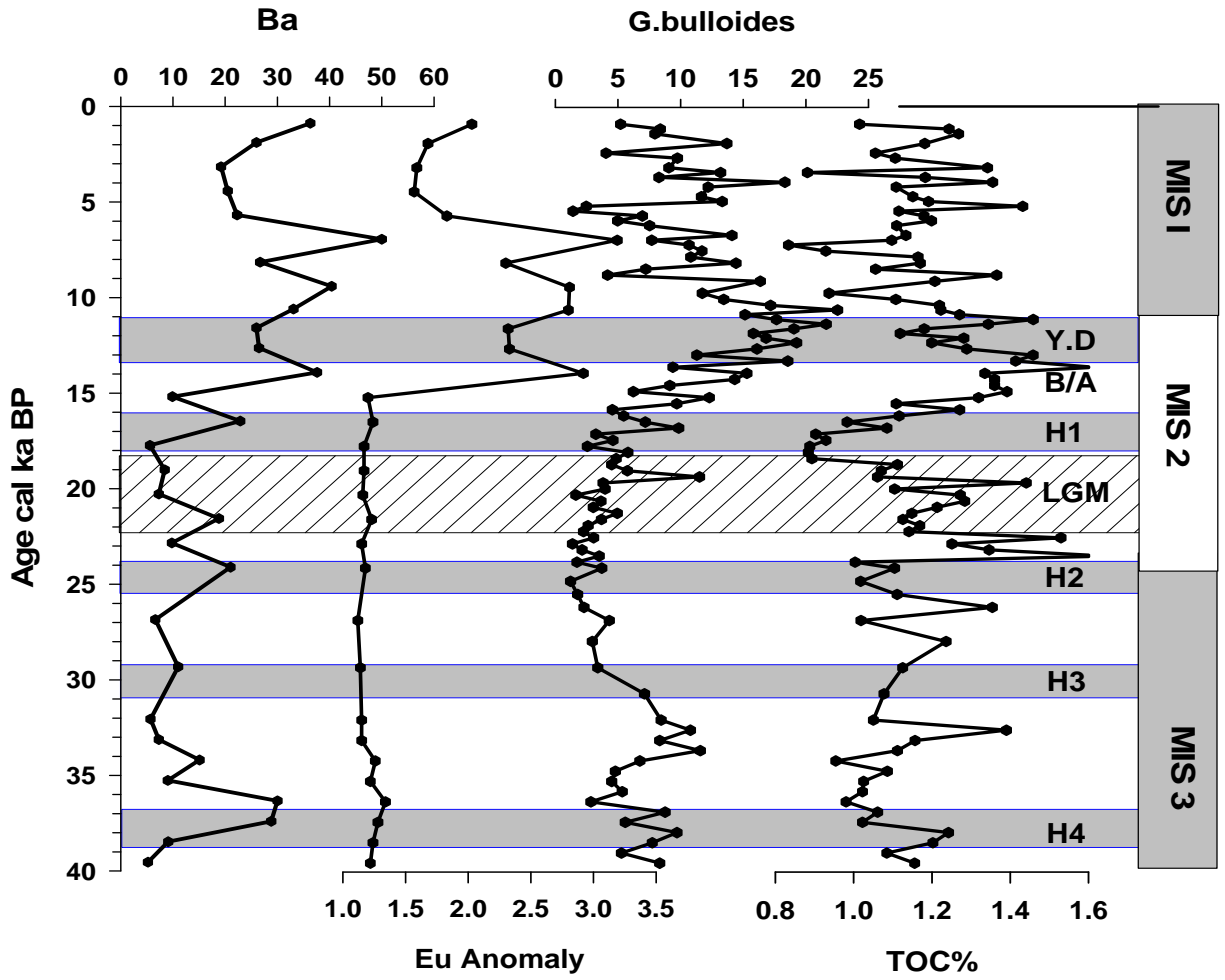


Fig. 5